Sirt1 enhances skeletal muscle insulin sensitivity in mice during caloric restriction

Simon Schenk,[1,2] Carrie E. McCurdy,[3] Andrew Philp,[4] Mark Z. Chen,[1] Michael J. Holliday,[3] Gautum K. Bandyopadhyay,[1] Olivia Osborn,[1] Keith Baar,[4] and Jerrold M. Olefsky[1]

[1]Division of Endocrinology and Metabolism, Department of Medicine, and [2]Department of Orthopaedic Surgery, UCSD, La Jolla, California, USA. [3]Department of Pediatrics, School of Medicine, University of Colorado Denver, Aurora, Colorado, USA. [4]Department of Neurobiology, Physiology, and Behavior, UCD, Davis, California, USA.

Skeletal muscle insulin resistance is a key component of the etiology of type 2 diabetes. Caloric restriction (CR) enhances the sensitivity of skeletal muscle to insulin. However, the molecular signals within skeletal muscle linking CR to improved insulin action remain largely unknown. Recently, the mammalian ortholog of *Sir2*, sirtuin 1 (Sirt1), has been identified as a potential transducer of perturbations in cellular energy flux into subsequent metabolic adaptations, including modulation of skeletal muscle insulin action. Here, we have demonstrated that CR increases Sirt1 deacetylase activity in skeletal muscle in mice, in parallel with enhanced insulin-stimulated phosphoinositide 3-kinase (PI3K) signaling and glucose uptake. These adaptations in skeletal muscle insulin action were completely abrogated in mice lacking Sirt1 deacetylase activity. Mechanistically, Sirt1 was found to be required for the deacetylation and inactivation of the transcription factor Stat3 during CR, which resulted in decreased gene and protein expression of the p55α/p50α subunits of PI3K, thereby promoting more efficient PI3K signaling during insulin stimulation. Thus, these data demonstrate that Sirt1 is an integral signaling node in skeletal muscle linking CR to improved insulin action, primarily via modulation of PI3K signaling.

Introduction

Skeletal muscle insulin resistance is a common metabolic disorder in obese and aged individuals and a key contributor to the etiology of type 2 diabetes (1). Moderate caloric restriction (CR; a 10%–40% reduction below ad libitum [AL] intake) enhances skeletal muscle insulin sensitivity and reverses insulin resistance in aged and obese skeletal muscle (2–8). However, the molecular signals within skeletal muscle linking CR to improved insulin action are incompletely defined. CR-induced improvements in insulin-stimulated glucose uptake by skeletal muscle in response to a physiological insulin concentration can be attributed to greater Glut4 recruitment to the cell surface (7). Complimenting this adaptation, a consistent finding is that CR augments Akt activation, particularly, Akt2 (3–5, 8, 9). Indeed, Akt2 is essential for the full effect of CR on skeletal muscle insulin sensitivity (3), and the phosphoinositide 3-kinase (PI3K) inhibitor, wortmannin, inhibits the ability of CR to increase skeletal muscle insulin sensitivity (6), which suggests that PI3K signaling contributes to improved insulin signaling after CR. However, most studies suggest that insulin-stimulated PI3K activity is not enhanced after CR (6, 9–11). Regardless, the molecular convergence point linking CR to enhanced insulin-stimulated PI3K-Akt signaling in skeletal muscle remains to be determined.

In recent years, the mammalian ortholog of *Sir2*, sirtuin 1 (Sirt1), has received significant attention as a key signaling node, linking perturbations in energy flux associated with CR (in particular, an increase in cellular NAD^+ and the NAD^+/NADH ratio) to subsequent cellular adaptations (12, 13). Sirt1 is a member of the conserved sirtuin family of NAD^+-dependent deacetylases and is necessary for the longevity effects of CR in simple organisms and rodents (12–14). Similarly, mice with transgenic overexpression of Sirt1 demonstrate a metabolic profile resembling that of CR (15). Considering that Sirt1 is sensitive to changes in NAD^+ and the NAD^+/NADH ratio and activation of Sirt1 can enhance skeletal muscle insulin sensitivity, the objective of this study was to investigate whether Sirt1 is the putative signaling node linking CR to enhanced skeletal muscle insulin signaling and sensitivity.

Results

Mouse model. To address the role of Sirt1 deacetylase activity in the enhancement of skeletal muscle insulin sensitivity with CR, we studied mice with KO of Sirt1 deacetylase activity in skeletal muscle, which we recently generated (16). These mice are referred to as mKO mice herein, and in these mice, exon 4 of the *Sirt1* gene, which encodes for the deacetylase domain of Sirt1, is deleted, and a shorter Sirt1 protein that is deacetylase inactive is expressed (refs. 16, 17, and Supplemental Figure 1A; supplemental material available online with this article; doi:10.1172/JCI58554DS1). For simplicity, we refer to the floxed mice ($Sirt1^{FloxExon4}$ mice) used to generate the mKO mice as WT mice herein. Deletion of exon 4 was specific to skeletal muscle in mKO mice and was equally efficient across various skeletal muscles (Supplemental Figure 1B).

Sirt1 deacetylase activity is not increased in mKO skeletal muscle with CR. We measured the acetylation status of p53 (Ac-p53) and peroxisome proliferator-activated receptor γ coactivator 1α (Ac-Pgc1α), known targets of Sirt1 (17–21), in muscle from 4-month-old WT and mKO mice fed an AL or CR (60% of AL intake) diet for 20 days. In skeletal muscle, Ac-p53 (Figure 1A) and Ac-Pgc1α (Figure 1B) were markedly reduced (~40%) in WT mice fed a CR diet (WT-CR mice) compared with those in WT mice fed an AL diet (WT-AL mice), but this reduction did not occur in mKO mice fed a CR diet (mKO-CR mice), confirming that Sirt1 deacetylase activity was increased by CR in WT mice but was ablated in muscle of mKO mice. There was no effect of genotype or diet on total Pgc1α or p53 abundance in skeletal muscle (Figure 1, A and B, bottom).

Conflict of interest: The authors have declared that no conflict of interest exists.
Citation for this article: *J Clin Invest.* 2011;121(11):4281–4288. doi:10.1172/JCI58554.

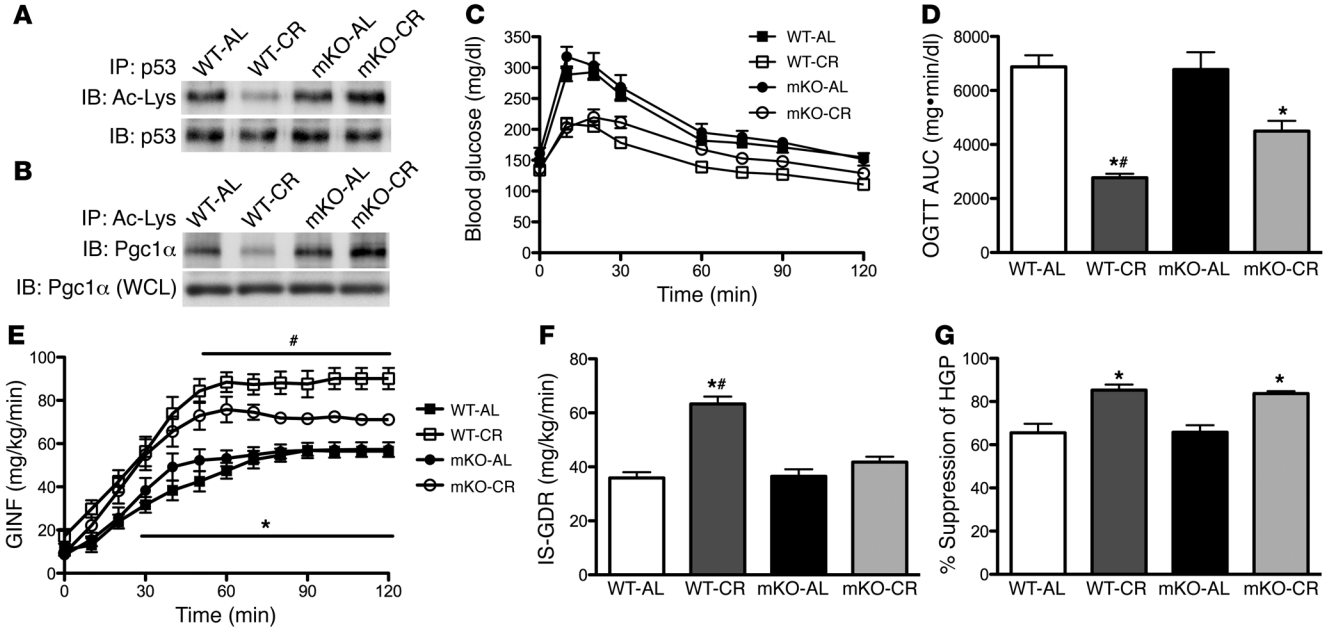

Figure 1

Skeletal muscle Sirt1 deacetylase activity modulates enhanced in vivo insulin action after CR. (**A**) Ac-p53 in skeletal muscle. p53 was immunoprecipitated from whole cell lysate (WCL) with anti-p53, and immunoprecipitates were immunoblotted with anti–acetyl lysine (Ac-Lys) and anti-p53. (**B**) Ac-Pgc1α in skeletal muscle. Acetylated proteins were immunoprecipitated from whole cell lysate with anti–acetyl lysine and immunoblotted for Pgc1α. Pgc1α was also measured in the whole cell lysate used for immunoprecipitation. (**C**) Blood glucose concentration and (**D**) area under the blood glucose curve (AUC) during an OGTT (1 g/kg). n = 8–10/group. (**E**) GINF, (**F**) IS-GDR, and (**G**) percentage suppression of HGP during a hyperinsulinemic-euglycemic clamp. n = 6–8/group. A 2-way ANOVA for main effects of diet and genotype was used for statistical analysis, with Tukey post-hoc test. $^{*}P < 0.05$, within same genotype; $^{\#}P < 0.05$, within same diet group. Data are mean ± SEM.

Improved in vivo insulin sensitivity after CR is attenuated in mKO mice. In response to CR, body weight decreased as expected, and this reduction was equal in both genotypes (Supplemental Figure 1C). The glycemic response to an oral glucose tolerance test (OGTT) was markedly reduced in WT-CR mice compared with that in WT-AL mice (Figure 1C), with an approximately 60% reduction in the AUC for the OGTT (Figure 1D). Glucose tolerance was also improved in the mKO-CR mice, although this improvement was attenuated as compared with that in WT-CR mice (Figure 1, C and D). In support of the OGTT data, the glucose infusion rate (GINF) during a hyperinsulinemic-euglycemic clamp (insulin infusion rate, 4 mU/kg/min) was increased by approximately 60% in WT-CR mice compared with that in WT-AL mice (Figure 1E). This improvement was due to increased skeletal muscle, liver, and adipose tissue insulin sensitivity, as measured by the insulin-stimulated glucose disposal rate (IS-GDR; Figure 1F), percentage suppression of hepatic glucose production (HGP; Figure 1G and Supplemental Figure 2A), and percentage suppression of free fatty acid (FFA) concentration (Supplemental Figure 2, B and C), respectively. In contrast, the CR-induced increase in GINF was markedly attenuated in mKO-CR mice (Figure 1E). This was solely due to an inability of CR to enhance IS-GDR (Figure 1F), as liver (Figure 1G and Supplemental Figure 2A) and adipose tissue (Supplemental Figure 2, B and C) insulin sensitivity were enhanced to the same degree as in WT-CR mice. Blood glucose and plasma insulin concentrations as well as the specific activity of ^{3}H-glucose during the glucose clamp studies were similar among groups (Supplemental Figure 2, D–F).

Improved skeletal muscle insulin sensitivity with CR is completely abrogated in mKO mice. To confirm the muscle-specific phenotype, we measured ex vivo basal and insulin-stimulated glucose transport in isolated soleus and extensor digitorum longus (EDL) muscles as well as isolated primary adipocytes. In WT mice, CR significantly enhanced (~3 fold) insulin-stimulated ^{3}H-2-deoxyglucose (2DOG) uptake (2DOGU; insulin 2DOGU – basal 2DOGU) in EDL and soleus muscles in response to a physiological insulin concentration (60 μU/ml [0.36 nM]) in WT mice, but, remarkably, this enhancement was completely abrogated in mKO mice (Figure 2A and Supplemental Figure 3, A and B). There was no difference in soleus and EDL insulin sensitivity between WT-AL mice and mKO mice fed an AL diet (mKO-AL mice) (Figure 2A and Supplemental Figure 3, A and B). Differences in insulin sensitivity were not due to changes in Glut4 expression, as we found no effect of diet or genotype on *Glut4* gene or Glut4 protein expression (Supplemental Figure 3, C and D). Thus, these results are fully consistent with the in vivo data from the OGTT and clamp studies. To verify the tissue-specific effect of loss of Sirt1 deacetylase activity, we measured basal and insulin-stimulated 2DOGU in primary adipocytes. Unlike the muscle 2DOGU data, adipocyte insulin sensitivity was enhanced equally by CR in mKO and WT mice, as compared with that in AL-fed mice (Figure 2B), again, consistent with the in vivo data showing preserved adipose tissue insulin sensitivity in mKO-CR mice.

Enhanced insulin-stimulated Akt and PI3K activation with CR is completely abrogated in mKO mice. Insulin-stimulated Akt-Ser^{473} phosphorylation (p-Akt^{Ser473}) and Akt-Thr^{308} phosphorylation (p-Akt^{Thr308}) in soleus muscle was increased approximately 4 to 5 fold in WT-CR mice, but this improvement was completely abrogated in mKO-CR mice (Figure 2C). Similarly, and in line with our Akt phosphorylation results, insulin-stimulated phosphorylation of As160 was enhanced in WT-CR mice but not in mKO-CR mice (Supplemental Figure 3E). We found no effect of CR or genotype on phosphorylation of

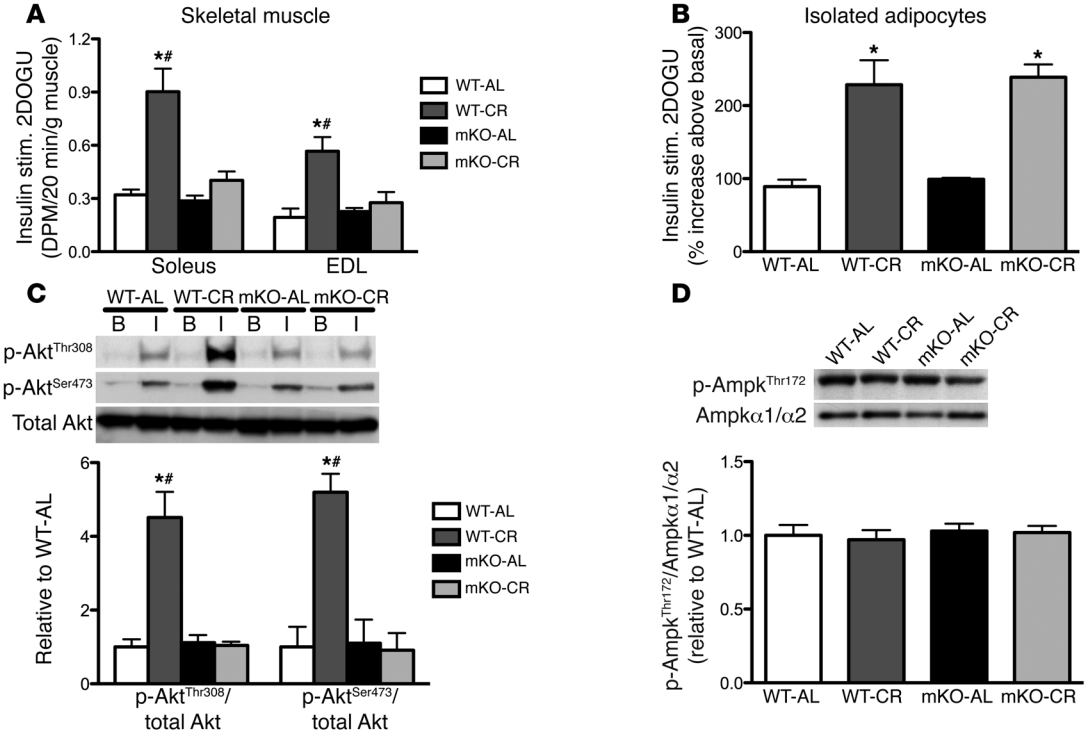

Figure 2

CR enhances ex vivo insulin-stimulated skeletal muscle glucose uptake and Akt phosphorylation in a Sirt1 deacetylase-dependent manner. (**A**) Insulin-stimulated (Insulin Stim.; 60 μU/ml) 2DOGU in isolated soleus and EDL muscles. Data are equal to insulin 2DOGU values minus basal 2DOGU values. DPM, disintegrations per minute. n = 6–8/group. (**B**) Percentage increase in 2DOGU above basal after insulin stimulation in isolated adipocytes. n = 5/group. (**C**) Representative blot of basal (B) and insulin-stimulated (I) phosphorylation of Akt (p-Akt^{Thr308}, p-Akt^{Ser473}, and total Akt) in isolated soleus muscles. Phosphorylation values are corrected for total Akt and are normalized to their respective basal value. Values are presented relative to WT-AL. n = 5/group. (**D**) Phosphorylation of Ampk (p-Ampk^{Thr172} corrected for Ampkα1/α2) in soleus muscle. n = 5/group. A 2-way ANOVA for main effects of diet and genotype was used for statistical analysis, with a Tukey post-hoc test. $^{*}P < 0.05$, within same genotype; $^{\#}P < 0.05$, within same diet group. Data are presented as mean ± SEM.

Ampk (p-Ampk^{Thr172}; Figure 2D). In addition, activation of Ampk, acetyl-CoA carboxylase (Acc), and 2DOGU in isolated EDL muscles by aminoimidazole carboxamide ribonucleotide (AICAR) was not different in WT mice versus mKO mice (Supplemental Figure 4, A–C). Since PI3K is a major upstream regulator of Akt, we focused on changes in PI3K function with CR. Similar to that in a recent CR study in rat skeletal muscle (5), p55α and p50α protein abundance was reduced approximately 30% in skeletal muscle of WT-CR mice, while p85α/β abundance was unchanged (Figure 3A). In contrast, no CR-induced reduction in p55α and p50α abundance occurred in mKO-CR muscle (Figure 3A). Consistent with the p-Akt and 2DOGU results, insulin-stimulated phosphotyrosine-associated PI3K activity was significantly enhanced in soleus muscle in WT-CR mice, but this enhancement was not observed in mKO-CR mice (Figure 3B).

Sirt1 modulates the expression of the p55α/p50α regulatory subunits of PI3K through deacetylation of Stat3. CR led to a significant (~40%) reduction in the acetylation status of Stat3 (Ac-Stat3) in skeletal muscle from WT mice, while this decrease did not occur in muscle from mKO-CR mice (Figure 3C). To further explore the effects of Ac-Stat3, we performed ChIP to quantify Stat3 binding to a consensus sequence in the p55α and p50α promoter regions of the *Pik3r1* gene, as previously described (22). Paralleling the Ac-Stat3 findings, Stat3 binding to p55α and p50α promoter regions was reduced approximately 80% in muscle from WT-CR mice compared with that from WT-AL mice, but this decrease did not occur in muscle from mKO-CR mice (Figure 3D). Assay background, as assessed by measuring binding to a nonspecific region in the *p85a* gene (upstream of the p50α promoter) was not different across groups (Figure 3D). Furthermore, input DNA for the ChIP analysis was not different across groups (Figure 3E). Complementing the ChIP findings, *p55a* and *p50a* mRNA levels were significantly decreased in WT-CR mice and not in mKO-CR mice (Figure 3F). There was no effect of genotype or diet on *p85a* mRNA levels.

Discussion

Greater efficiency of insulin signaling underlies enhanced skeletal muscle insulin sensitivity after CR (2–8), although the molecular signals linking CR to improved insulin action are incompletely defined. In this study, we demonstrated that 20 days of CR enhances skeletal muscle insulin sensitivity, secondary to increased insulin-stimulated PI3K activity, and that these adaptations occur in a Sirt1 deacetylase activity-dependent manner. Specifically, our results suggest that CR augments skeletal muscle PI3K signaling efficiency and insulin action via Sirt1-mediated deacetylation of Stat3, which modulates transcription of the p55α/p50α regulatory subunits of PI3K. Taken together, these results identify Sirt1 as a key molecular convergence point that links reduced nutrient intake during CR to improvements in skeletal muscle insulin sensitivity.

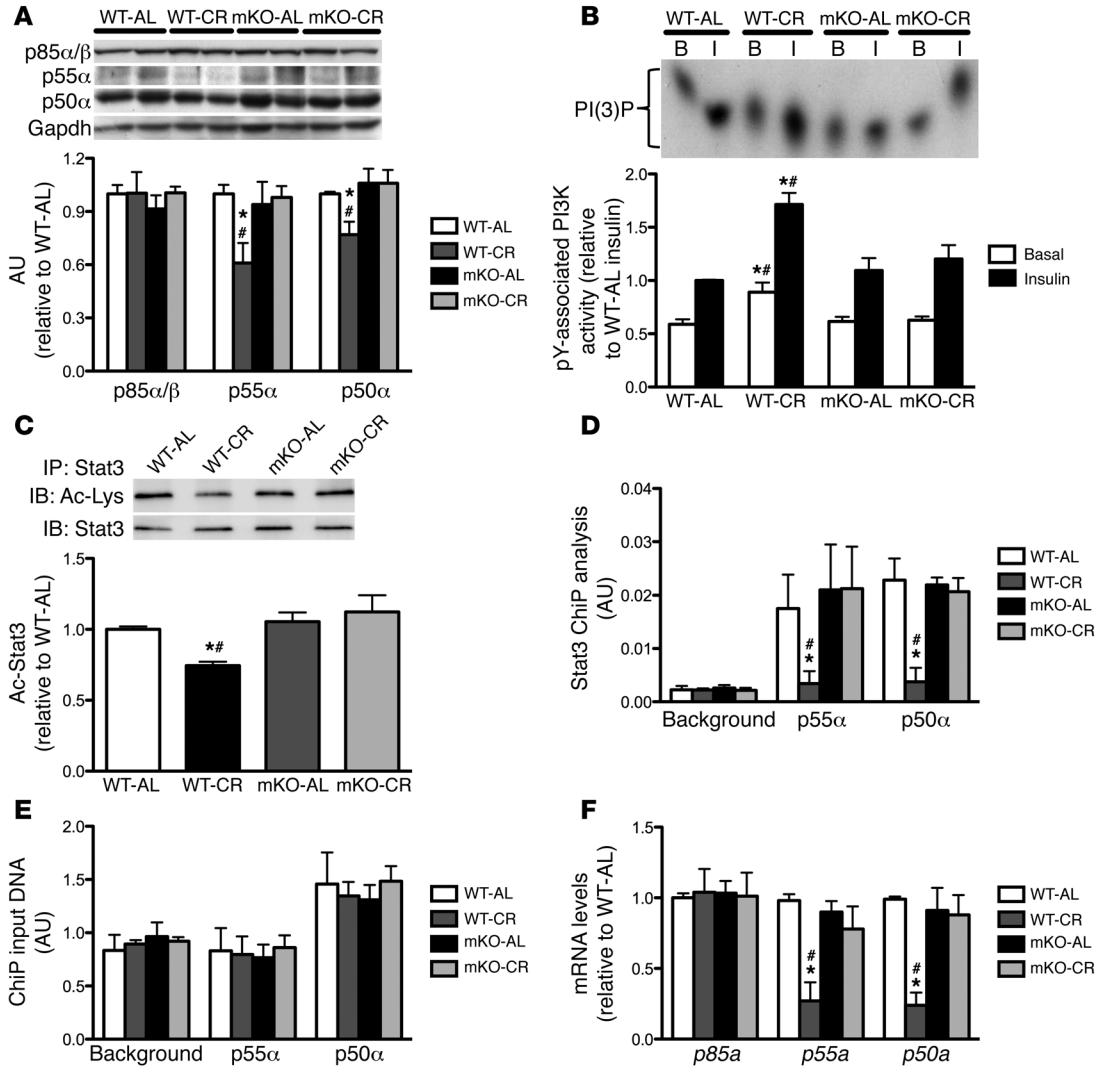

Figure 3

CR reduces the expression of the p55α/p50α regulatory subunits of PI3K and enhances insulin-stimulated PI3K activation in skeletal muscle via Sirt1-mediated Stat3 deacetylation. (**A**) Protein expression of the p85α/β, p55α, and p50α regulatory subunits of PI3K and Gapdh in soleus muscle. *n* = 5–6/group. (**B**) Basal and insulin-stimulated phosphotyrosine-associated (pY-associated) PI3K activity (*n* = 6–7/group) in soleus muscles. Note that in this image phosphoinositol 3-phopshate [PI(3)P] levels for insulin-stimulated KO AL muscle are less than those in the insulin-stimulated WT AL muscle. However, when the data are averaged across all samples and statistical analysis is performed, the data are as presented. (**C**) Acetylated Stat3 (*n* = 5/group), (**D**) Stat3 binding to a nonspecific region of the *p85a* gene upstream of the p50α start site (background) and the p55α and p50α promoters in the *p85a* gene, as measured by ChIP (*n* = 4/group), (**E**) input DNA for ChIP analysis, and (**F**) mRNA levels of *p85a*, *p55a*, and *p50a* (*n* = 6–7/group) in skeletal muscle. A 2-way ANOVA for main effects of diet and genotype was used for statistical analysis, with a Tukey post-hoc test. For PI3K activity, statistical analysis was conducted within the basal group only or within the insulin group only. $^{*}P < 0.05$, within same genotype; $^{\#}P < 0.05$, within same diet group. Data are presented as mean ± SEM.

Enhanced insulin-stimulated glucose uptake after brief CR is due to greater Glut4 recruitment to the cell surface (7) and is paralleled by changes in insulin signaling, particularly at the level of PI3K-Akt (3–5, 8, 9), and As160, a key downstream target of Akt (9). Indeed, studies using the PI3K inhibitor, wortmannin (6), and mice with KO of Akt2 (3), reveal that PI3K and Akt2 are essential for the ability of brief CR to enhance skeletal muscle insulin sensitivity. In contrast, CR does not appear to augment insulin action upstream of PI3K at the level of the IR or Irs1 in response to submaximal insulin (9) but has been shown to enhance IR-Irs1 activation in response to supraphysiological insulin stimulation (8, 9, 11, 23), although this is not a universal finding (24, 25). In addition, mice with KO of Irs1 exhibit the expected increase in skeletal muscle insulin sensitivity after CR (26). In this study, CR augmented insulin-stimulated PI3K-Akt-As160 signaling and 2DOGU in skeletal muscle from WT mice but not in that from mKO mice. However, increased insulin sensitivity was observed in other important metabolic tissues, such as liver and adipose tissue, in both mKO and WT mice. Thus, our results and those of Davidson et al. (6) demonstrate that greater insulin-stimulated PI3K signaling is essential for the functional improvements in Akt-As160 activity and glucose transport in

skeletal muscle after CR. Furthermore, our studies identify Sirt1 as a key orchestrator of these CR-mediated adaptations.

To date, the effects of CR on insulin-stimulated PI3K activity have been variable. Long-term (4 years) CR in cynomolgus monkeys enhanced insulin-stimulated PI3K activity under supraphysiological insulin concentrations during a hyperinsulinemic-euglycemic clamp (8). Additionally, brief CR augmented insulin-stimulated Irs1-p110 association (which is indicative of increased PI3K function) in response to supraphysiological (500 μU/ml) insulin in rat skeletal muscle, although PI3K activity was not directly determined (5). In contrast, a number of rodent studies have found no effect of brief (6, 10, 11) or longer-term (9) CR on insulin-stimulated PI3K activity in response to submaximal or maximal insulin stimulation. Our results clearly demonstrated that CR augments insulin-stimulated PI3K activity in response to a physiological insulin concentration (60 μU/ml) as well as Akt-As160 signaling and glucose transport. The discrepancy between our results and previous studies is likely due to the duration of insulin stimulation. Since PI3K activity rapidly increases and returns toward prestimulation levels after insulin (27), we measured PI3K activity in soleus muscles that were exposed to insulin for only 10 minutes. Other studies typically use 40–50 minutes (6, 9–11), and, therefore, peak insulin-stimulated PI3K activity may have been missed.

Based on our PI3K findings, we studied potential mechanisms for enhanced PI3K function. PI3K is a heterodimer comprising a p110α/β catalytic subunit bound to one of the PI3K regulatory subunits, p85α, p55α, p50α, or p85β (28). These regulatory subunits can bind as nonfunctional monomers to IRS proteins and attenuate insulin signaling, and, in line with this, a reduction in the abundance of any of the regulatory subunits improves insulin sensitivity (28–33), although complete loss of the regulatory subunits causes skeletal muscle insulin resistance (33). We found that the protein abundance of p55α/p50α in skeletal muscle was reduced by approximately 30% in WT mice after CR, which is comparable to a study in rat skeletal muscle (5). This reduction, however, did not occur in mKO mice after CR and, thus, provides a mechanism for the failure of CR to improve insulin-stimulated PI3K activity and skeletal muscle insulin sensitivity in mKO mice. Notably, a previous study found that skeletal muscle insulin-stimulated PI3K activity was not augmented in mice with complete KO of p55α/p50α (32). This disparity is likely due to the fact that complete ablation of p55α and p50α would reduce the absolute number of functional (i.e., p110-bound) PI3K available, and at the maximal insulin concentration used by the authors, phosphotyrosine-associated PI3K activity would be reduced. However, at the physiological insulin dose used in our study, we hypothesize that the modest but significant decrease in p55α/p50α reduces the potential binding of inhibitory monomers to IRS proteins with insulin stimulation, thus facilitating the binding of functional PI3K heterodimers.

Expression of the p55α and p50α transcripts of *Pik3r1* is regulated by the binding of Stat3 to the p55α and p50α promoters in the *Pik3r1* gene in a mammary gland development model (22). Interestingly, Stat3 acetylation regulates its ability to bind to the promoter regions of target genes, and Stat3 deacetylation is controlled by Sirt1 (34). Our immunoprecipitation and ChIP studies in WT and mKO mice indicate that CR modulates the protein abundance of p55α and p50α, at least in part by Sirt1-mediated deacetylation of Stat3, and reduced binding of Stat3 to the p55α and p50α promoters. It is notable that we found larger differences in the degree of change of *p55a/p50a* mRNA levels compared with the degree of change of p55α/p50α protein abundance. While the mechanism for this is not readily apparent, it may be due to differences in translation efficiency, protein stability, or protein degradation of p55α and p50α.

Mechanisms other than Sirt1/Stat3-mediated regulation of p55α/p50α and PI3K may contribute to improved skeletal muscle insulin action with CR. For example, Stat3 can be an adaptor molecule for p85α and subsequent type I interferon receptor signaling (35); however, another study suggests that IRS proteins, but not Stat3, are needed for activation of PI3K (36). Sirt1 may also mediate PI3K function during CR through binding to p85α (37) or insulin signaling via regulation of protein tyrosine phosphatase 1B expression (38). In addition, CR increases the association of heat shock protein 90 with Akt in skeletal muscle (9), which may facilitate Akt phosphorylation by reducing dephosphorylation of Akt by protein phosphatase 2A (39). Interestingly, lysine acetylation of the PH domain of Akt was recently shown to regulate Akt activity, and Sirt1 was shown to deacetylate Akt and enhance Akt activation (40). Deacetylation of Akt in response to serum stimulation also required PI3K (40), which perhaps suggests a model in which Sirt1 coordinately regulates PI3K and Akt during CR.

Interestingly, glucose tolerance and whole-body and muscle-specific insulin sensitivity were not impaired in mKO-AL mice compared with those in WT-AL mice, suggesting that loss of Sirt1 deacetylase activity in skeletal muscle is not detrimental to glucose homeostasis or muscle insulin action in young mice. Several studies have demonstrated that overexpression of Sirt1 in skeletal muscle or in C2C12 muscle cells does not augment insulin-stimulated glucose uptake under normal conditions, despite increased Sirt1 activity (38, 41). Conversely, loss of Sirt1 deacetylase activity in 293 cells and L6 myoblasts impairs insulin-stimulated Akt phosphorylation, although whether this has functional effects on glucose transport was not assessed (37). Irrespective, our ex vivo studies demonstrate that loss of Sirt1 in skeletal muscle does not impair insulin-stimulated Akt activation or glucose transport in the AL-fed mice in response to a physiological insulin concentration. Since Sirt1 is sensitive to perturbations in NAD^+, we hypothesize that in the AL-fed condition macronutrient supply to the myocyte is adequate, and thus the NAD^+/NADH ratio is not perturbed, and Sirt1 is not activated. This is supported by the fact that Ac-p53 and Ac-Pgc1α are not increased in mKO-AL muscle.

Ampk is an important regulator of glucose uptake in skeletal muscle, and functional Ampk is required for the activation of Sirt1 during energy depletion and in response to exercise, via modulation of NAD^+ metabolism (42, 43). Nevertheless, a number of studies have found that Ampk activity and downstream signaling are not augmented in skeletal muscle with CR (3, 9, 44), although this is not a universal finding (45). It should be noted that CR increases Ampk activity in other tissues, such as heart and liver (46–48), and these differences may represent tissue-specific effects of CR and Ampk. We also found no effect of CR on Ampk activation, and we recently demonstrated that exercise-induced activation of Ampk does not require functional Sirt1 deacetylase activity (16). Moreover, herein, we demonstrate that Ampk/AICAR-mediated glucose transport does not require functional Sirt1 deacetylase activity, although whether Ampk-mediated activation of glucose transport during CR requires Sirt1 deacetylase activity was not addressed.

In summary, herein we demonstrated that CR has systemic effects to improve insulin sensitivity in major insulin target tissues, but in the absence of functional Sirt1 deacetylase activity in skeletal muscle, the ability of CR to enhance skeletal muscle insulin sensitivity is lost. The cellular mechanisms involve an increase in the overall efficiency of insulin-stimulated PI3K signaling, secondary to Sirt1-mediated

deacetylation of Stat3 and a reduction in the expression of the p55α/p50α regulatory subunits of PI3K. Taken together, these data illustrate a mechanism which we believe to be novel, whereby SIRT1 regulates enhanced insulin-stimulated skeletal muscle glucose disposal in response to CR via its ability to detect changes in nutrient flux and transduce these signals into more efficient PI3K signaling.

Methods

Animals. Mice were on a C57BL/6 background, and all studies were conducted in male mice. Generation of the muscle-specific, Sirt1 deacetylase-inactive mice (mKO mice) has been described previously (16). Briefly, mice harboring loxP sites flanking exon 4 of the *Sirt1* gene (Sirt1^{FloxExon4} mice) (17) (provided by Fred W. Alt [Howard Hughes Medical Institute and Harvard Medical School, Boston, Massachusetts, USA] and David S. Lombard [University of Michigan, Ann Arbor, Michigan, USA]), which encodes the deacetylase domain of Sirt1, were crossed with mice expressing Cre recombinase under the control of the muscle creatine kinase promoter. These mice are referred to as mKO mice. For simplicity, the SIRT^{FloxExon4} mice are referred to as WT mice and were used as the control (i.e., WT) mouse. For measurement of exon 4 in the various skeletal muscles, adipose tissue, and liver, a standard PCR protocol was used on a Bio-Rad MyCycler thermal cycler, and products were run on a 2% agarose gel and were then visualized. The following primers were used for PCR analysis: exon 3 of *Sirt1* gene, 5′-GATGCTGTGAAGTTACTGCAGGAGTG-3′; exon 5 of *Sirt1* gene, 5′-AATTTGTGACACAGAGACGGCTGG-3′. For major outcome measurements, different groups of mice were used for clamp and ex vivo insulin stimulation studies. All measurements were performed between 1100 and 1300 hours. For these experiments, WT mice were fasted for 4 to 6 hours, while CR mice received their food at 1700 hours the previous day. Importantly, studies have demonstrated that the timing of feeding before beginning the fast and duration of fast during CR do not effect measurement of skeletal muscle insulin sensitivity (49). Mice were housed on a 12 -hour-light/12-hour-dark cycle. All experiments were approved by and were conducted in accordance with the Animal Care Program at UCSD.

CR diet. Mice were group housed until 8 weeks of age and then were placed in individual housing. At 9 weeks of age, AL food intake of normal chow (LabDiet no. 5001) diet was measured daily (at 1700 hours) for 7 days. At 10 weeks of age, mice (a) continued AL diet intake or (b) were switched to a CR (60% of AL intake) diet. Body weight and food intake were measured daily at 1700 hours, and food was provided at this time for CR mice. Mice remained on AL or CR diet for an additional 20 days (~13 weeks of age).

OGTT. On day 15 after initiating CR or continuing AL diet, fasted (4 hours) mice were orally gavaged with 12.5% dextrose (1 g/kg; Hospira Inc.). Blood glucose was measured (OneTouch Ultra 2, Lifescan Inc.) at 0, 10, 20, 30, 60, 75, 90, and 120 minutes after gavage.

Hyperinsulinemic-euglycemic clamps. Clamps were conducted in chronically cannulated, conscious, fasted (6 hours) mice as previously described (50). Cannulation was performed in anesthetized (ketamine [80 mg/kg], acepromazine [0.5 mg/kg], and xylazine [16 mg/kg]) mice 4–5 days before the clamp measurement. For the clamp, the insulin (Humulin R, Eli Lilly and Company) infusion rate was 4 mU/kg/min. [3-^{3}H] D-glucose (5 Ci/h; PerkinElmer) was infused in order to calculate HGP/insulin sensitivity and skeletal muscle insulin sensitivity (IS-GDR). Blood glucose concentration was clamped at 120 mg/dl. In addition to blood collected for tracer analysis (15 μl in duplicate for each time point, i.e., 0, 110, and 120 minutes), blood (75 μl) was collected before and after the clamp for measurement of plasma insulin (Alpco Diagnostics) and FFA (Wako Pure Chemical Industries Ltd.) concentrations.

Isolated skeletal muscle insulin stimulation. Ex vivo muscle insulin sensitivity was measured by the 2DOGU technique (3). Fasted (4 hours) mice were anesthetized (150 mg/kg Nembutal) via intraperitoneal injection. Paired soleus and EDL muscles were incubated at 35°C for 30 minutes in oxygenated (95% O_2, 5% CO_2) flasks of Krebs-Henseleit buffer (KHB) containing 0.1% BSA, 2 mM Na-pyruvate, and 6 mM mannitol. For 2DOGU analysis, 1 muscle per pair was incubated in KHB without insulin, and the contralateral muscle was incubated in KHB with insulin (60 μU/ml [0.36 nM]; Humulin R, Eli Lilly and Company). After 30 minutes, muscles were transferred to a second flask and incubated at 35°C for 20 minutes in KHB plus 0.1% BSA, 9 mM [^{14}C]-mannitol (0.053 mCi/mmol; PerkinElmer), and 1 mM [^{3}H]-2DG (6 mCi/mmol; PerkinElmer), with the same insulin concentration as in the first incubation. Because PI3K activity peaks and returns to baseline readily after insulin stimulation (27), for samples used to assess phosphotyrosine-associated PI3K activity during the initial 30-minute incubation, in a separate group of mice, muscle pairs were incubated in the same incubation media, but no insulin was included with either pair. After 30 minutes, muscles were then incubated without or with (60 μU/ml) insulin for 10 minutes, and no radioactive tracer was used. After the second incubation phase, muscles were blotted on ice-cold filter paper, trimmed, freeze-clamped, and then stored (−80°C). 2DOGU rate was calculated as previously described (3). The soleus muscles used for 2DOGU measurements (i.e., 50 minutes without or with insulin stimulation) were used to measure phosphorylation of Akt (p-Akt^{Ser473}, p-Akt^{Thr308}), As160 (phospho-Akt substrate–As160 [PAS-As160]), and p85α/p85β/p55α/p50α abundance, as described below (see *As160 phosphorylation* and *SDS-PAGE*).

Isolated adipocyte glucose uptake. In a subset of mice from skeletal muscle 2DOGU studies, we isolated the epididymal fat pad to measure basal and insulin-stimulated glucose transport in isolated adipocytes, adapting the protocol of Karnieli et al. (51). Briefly, Krebs-Ringer bicarbonate-HEPES (KRBH) buffer, pH 7.4, containing 10 mM bicarbonate, 30 mM HEPES, 200 nM adenosine, 2.5 mM glucose, and 1% fatty acid–free BSA was used as an incubation medium. In a 50-ml polycarbonate tube, the epididymal fat pads were mixed with 5 ml KRBH and 25 mg collagenase (type I) and gently rocked at 37°C. After 30 to 40 minutes, the digestion mixture was filtered through a nylon strainer and centrifuged at 400 *g* for 1 minute. The floating fat cells were isolated and washed 3 times with warm KRBH. A 25%–30% (vol/vol) suspension of fat cells in glucose-free KRBH was then used to study basal and insulin-stimulated uptake of ^{3}H-2DOG. For this, cells were pretreated with and without insulin for 20 minutes and incubated at 37°C with 0.1 mM [^{3}H]-2DOG (6 mCi/mmol; 0.4 mCi/ml; PerkinElmer) for 10 minutes. Immediately after incubation, the suspension was loaded on top of 0.2 ml silicon oil inside a long, narrow 0.4-ml polyethylene tube and centrifuged (10,000 *g* for 10 seconds). The fat cells were then isolated, and the level of radioactivity was counted. An aliquot of the suspension was used to determine cell number, and uptake was corrected for cell number.

AICAR studies. For AICAR studies, 2DOGU was measured in isolated EDL muscles from WT and mKO mice (13 weeks old) using the protocol described above for insulin stimulation, except insulin was not used. Briefly, paired EDL muscles were excised from fasted (4 hours) and anesthetized (150 mg/kg Nembutal) mice and were incubated at 35°C for 30 minutes in oxygenated (95% O_2, 5% CO_2) flasks of KHB containing 0.1% BSA, 2 mM Na-pyruvate, and 6 mM mannitol. One muscle per pair was incubated in KHB without AICAR, and the contralateral muscle was incubated in KHB with AICAR (2 mM; EMD Chemicals Inc., catalog no. 123041). After 30 minutes, muscles were transferred to a second flask and incubated at 35°C for 20 minutes in KHB plus 0.1% BSA, 9 mM [^{14}C]-mannitol (0.053 mCi/mmol; PerkinElmer), and 1 mM [^{3}H]-2DG (6 mCi/mmol; PerkinElmer) with the same AICAR concentration as in the first incubation. After the second incubation phase, muscles were blotted on ice-cold filter paper, trimmed, freeze-clamped, and then stored (−80°C). 2DOGU rate was calculated as previously described (3). Activation of Ampk and Acc was measured in the same muscles.

Measurement of protein acetylation. Protein acetylation was assessed in gastrocnemius muscle as previously described (16). Briefly, 200 μg of protein lysate was precleared with protein A and G agarose beads (Millipore, catalog no. 16-156

and 16-266), and protein was then rotated for 2 hours (4°C) with anti–Ac-Lys (Cell Signaling Technology, catalog no. 9441), anti-p53 (Santa Cruz Biotechnology, catalog no. 482), anti-Pgc1α (Millipore, AB3242), or anti-Stat3 (Santa Cruz Biotechnology, catalog no. 6243). Then, protein A and G agarose beads (Millipore, catalog no. 16-156 and 16-266) were added, and the samples were rotated overnight (4°C). The following morning agarose beads were washed 6 times (3 times in buffer A, 1% NP-40 and 0.1 mM Na_3VO_4 in PBS, and 3 times in buffer B, 0.01 M Tris, pH 7.5, 1 mM EDTA, 0.1 M NaCl, and 0.1 mM Na_3VO_4 in PBS). Antigens were eluted from the beads with 1x SDS buffer and were boiled for 5 minutes before separation using standard SDS-PAGE methods.

As160 phosphorylation. Lysate (125 μg) from basal and insulin-stimulated soleus muscles used for 2DOGU analysis was rotated with anti-As160 (gift from Graham Hardie, University of Dundee, Dundee, United Kingdom) for 2 hours, and then protein A agarose beads (Millipore, catalog no. 16-156) were added, and the samples were rotated overnight (4°C). The following morning agarose beads were washed 6 times (3 times in buffer A and 3 times in buffer B; see above). Antigens were eluted from the beads with 1x SDS buffer and were boiled for 5 minutes before separation using standard SDS-PAGE methods.

SDS-PAGE. SDS-PAGE was performed on 7.5% tris-acetate gels using standard methods, as previously described (16). Primary antibodies used for immunoblotting were from Cell Signaling Technology (p-Ampk^{Thr172}, catalog no. 2531; p-Akt^{Ser473}, catalog no. 9271; p-Akt^{Thr308}, catalog no. 9275; Akt, catalog no. 9272; Ac-Lys, catalog no. 9441; p53, catalog no. 2524; PAS, catalog no. 9611; p-Acc^{Ser79}, catalog no. 3661; Acc, catalog no. 3662), Millipore (Pgc1α, catalog no. AB3242; pan-p85, catalog no. 06-195), and Santa Cruz Biotechnology (Glut4, catalog no. 7938; Gapdh, catalog no. 20357). Antibodies for Ampk1/2 and As160 were provided by Graham Hardie.

PI3K activity. PI3K was immunoprecipitated from 300 μg of basal and insulin-stimulated (10 minutes) soleus muscle protein by incubating overnight with a rabbit anti-phosphotyrosine antibody (Cell Signaling Technology, catalog no. 9411). The following morning samples were incubated for 2 hours with 50 μl protein A agarose beads (Millipore, catalog no. 16-156) and were washed as previously described (52). The kinase reaction was initiated with the addition of 2 μg phosphatidylinositol and 20 μCi [γ-^{32}P]-ATP and was allowed to proceed for 30 minutes. After termination of the reaction by the addition of 20 μl 8 N HCL, the lipid products were separated from the remaining [γ-^{32}P]-ATP with 2 successive chloroform extractions and then run for 2 hours on a thin-layer chromatography plate. Separated PI(3)P was visualized on film.

ChIP assay. ChIP experiments were performed using a commercially available kit according to the manufacturer's instructions (EZ-ChIP; Millipore, catalog no. 17-295). Briefly, 100 mg powdered gastrocnemius muscle was rotated end over end for 10 minutes in 10 ml ice-cold 1% high-grade formaldehyde/PBS solution. Cross-linking was stopped with the addition of 1 ml ice-cold glycine, and samples were left to stand on ice for 10 minutes. Cross-linked muscle was pelleted via centrifugation (5,000 *g*/4°C for 5 minutes) and washed 3 times with ice-cold PBS (5 ml). After the final wash, muscle samples were transferred to a 1.5-ml eppendorf tube and homogenized in 250 μl of 20% SDS lysis buffer containing protease inhibitor cocktail II (Sigma-Aldrich, catalog no. P5726), using a hand-held micro homogenizer (Bio-Gen PRO200). Homogenates were sonicated on ice (four 10-second pulses separated by 1 minute), and the protein content was measured via the DC protein assay (Bio-Rad). One mg DNA/protein complex was suspended in 1 ml of dilution buffer and precleared with 30 μl protein A sepharose beads for 1 hour at 4°C with rotation. Samples were then transferred to new tubes and immunoprecipitated overnight at 4°C with rotation using 8 μl anti-Stat3 antibody (Santa Cruz Biotechnology, catalog no. sc-482) or 8 μl rabbit IgG antibody as a control (Thermo Scientific, catalog no. 31430). The following day, DNA/protein complexes were washed 5 times, eluted from sepharose beads, and then reverse cross-linked overnight at 65°C. The next day, DNA was extracted using spin filter columns according to the kit instructions (EZ-ChIP; Millipore, catalog no. 17-295). Input and bound DNA was detected by real-time quantitative PCR (RT-qPCR) as previously described (22). Briefly, specific primers were used to amplify a 297-bp region (–244 bp to –541 bp) spanning the Stat3 binding site (–276 bp) in the mouse p50α promoter or a 260-bp region (–375 bp to 635 bp) spanning the Stat3 binding site (–624 bp) in the mouse p55 promoter. Assay background was determined using primers to amplify a product of 146 bp in a nonspecific region of the *p85a* gene upstream of the p50α start site (–7,130 bp to –7,282 bp from p50α transcription start site). The sequences used for RT-PCR analysis are as follows: p50α, 5′-GTGGCCGAGGCAAGACTAAC-3′ and 5′-CTGCGGGGCTGACTGTG-3′; p55α, 5′-ATCAGATATCCCAAGGTCAAAACAAGA-3′ and 5′-ACCTTCCTTAAAGCAGCTAGCAATGAG-3′; background, 5′-GGCCACTCATCAGCTCTCACCCATAC-3′ and 5′-GCTCTCTCAAGCCTCCAGCAAAAACC-3′.

RT-qPCR analysis. RNA was extracted from skeletal muscle (gastrocnemius, soleus, plantaris, EDL), liver, or adipose tissue using the phenol/chloroform method as previously described (16). RNA was quantified using a NanoDrop 1000 spectrophotometer (Thermo Scientific) at 260 and 280 nm. First-strand cDNA was synthesized (Bio-Rad) from 1 μg RNA using the Reverse Transcription System (Promega) according to the manufacturer instructions. RT-qPCR was performed to measure relative mRNA expression using an Eppendorf LightCycler PCR machine, SYBR Green PCR plus reagents (Sigma-Aldrich), and custom designed primers. Ten μl PCR reactions were assayed in triplicate on a 96-well heat-sealed PCR plate (Thermo Scientific). Each reaction contained 5 μl SYBR Green Taq Polymerase (Sigma-Aldrich, catalog no. S4438), 1 μl of forward and reverse primers, and 3 μl cDNA (1:10 dilution). The target gene expression for each sample was calculated relative to GAPDH, and values are presented normalized to WT-AL values. Absolute C_T for Gapdh was unchanged by any of the treatments. Primers for RT-PCR were designed to span exon-exon boundaries to avoid amplification of genomic DNA. The following primer sequences were used: *p85a*, 5′-AGGGAAGAGGTGAATGAGAG-3′ and 5′-TTGGACACAGGGTAGAGAAG-3′; *p55a*, 5′-AGCAAAGCCAAGGAAACTG-3′ and 5′-GTGCTGGTGGATCCATTTCT-3′; *p50a*, 5′-GCTGGGACCACTTGGTAGAA-3′ and 5′-GGGCAGTGTTTGCAGGTTAT-3′; *Glut4*, 5′-ACTCTTGCCACACAGGCTCT-3′ and 5′-CCTTGCCCTGTCAGGTATGT-3′; *Gapdh*, 5′-TGGAAAGCTGTGGCGTGAT-3′ and 5′-TGCTTCACCACCTTCTTGAT-3′.

Statistics. Statistical analyses were performed using SigmaPlot 11.2 (Systat Software Inc.). Data were analyzed by a 2-way ANOVA (with repeated measures when necessary) for main effects of diet and genotype, followed by a Tukey post-hoc analysis, with significant differences at $P < 0.05$. All data are expressed as mean SEM.

Acknowledgments

We thank Fred W. Alt and David S. Lombard for sharing the floxed mice and their expertise. We thank Christine Watson (University of Cambridge, Cambridge, United Kingdom) for helpful advice with ChIP experiments. This work was supported by grants from the NIH (DK033651, DK074868, T32 DK007494, DK063491, U54 HD012303-25, R24 HD050837, P30 AR058878-02, and UL1 RR024146). S. Schenk was supported in part by a Mentor-Based Postdoctoral Fellowship from the American Diabetes Association awarded to J.M. Olefsky, and C.E. McCurdy is supported in part by a grant from the NIH (K12 HD057022).

Received for publication April 18, 2011, and accepted in revised form September 7, 2011.

Address correspondence to: Jerrold M. Olefsky, Department of Medicine, University of California, San Diego, 9500 Gilman Drive, La Jolla, California 92093-0673, USA. Phone: 858.534.6651; Fax: 858.534.6653; E-mail: jolefsky@ucsd.edu.

1. Lillioja S, et al. Insulin resistance and insulin secretory dysfunction as precursors of non-insulin-dependent diabetes mellitus. Prospective studies of Pima Indians. *N Engl J Med*. 1993;329(27):1988–1992.
2. Cartee GD, Kietzke EW, Briggs-Tung C. Adaptation of muscle glucose transport with caloric restriction in adult, middle-aged, and old rats. *Am J Physiol*. 1994;266(5 pt 2):R1443–R1447.
3. McCurdy CE, Cartee GD. Akt2 is essential for the full effect of calorie restriction on insulin-stimulated glucose uptake in skeletal muscle. *Diabetes*. 2005; 54(5):1349–1356.
4. McCurdy CE, Davidson RT, Cartee GD. Brief calorie restriction increases Akt2 phosphorylation in insulin-stimulated rat skeletal muscle. *Am J Physiol Endocrinol Metab*. 2003;285(4):E693–E700.
5. McCurdy CE, Davidson RT, Cartee GD. Calorie restriction increases the ratio of phosphatidylinositol 3-kinase catalytic to regulatory subunits in rat skeletal muscle. *Am J Physiol Endocrinol Metab*. 2005;288(5):E996–E1001.
6. Davidson RT, Arias EB, Cartee GD. Calorie restriction increases muscle insulin action but not IRS-1-, IRS-2-, or phosphotyrosine-PI 3-kinase. *Am J Physiol Endocrinol Metab*. 2002;282(2):E270–E276.
7. Dean DJ, Brozinick JT Jr, Cushman SW, Cartee GD. Calorie restriction increases cell surface GLUT-4 in insulin-stimulated skeletal muscle. *Am J Physiol*. 1998; 275(6 pt 1):E957–E964.
8. Wang ZQ, et al. Modulation of skeletal muscle insulin signaling with chronic caloric restriction in cynomolgus monkeys. *Diabetes*. 2009;58(7):1488–1498.
9. Sharma N, et al. Mechanisms for increased insulin-stimulated Akt phosphorylation and glucose uptake in fast- and slow-twitch skeletal muscles of calorie restricted rats. *Am J Physiol Endocrinol Metab*. 2011;300(6):E966–E978.
10. Dean DJ, Cartee GD. Brief dietary restriction increases skeletal muscle glucose transport in old Fischer 344 rats. *J Gerontol A Biol Sci Med Sci*. 1996; 51(3):B208–B213.
11. Dean DJ, Cartee GD. Calorie restriction increases insulin-stimulated tyrosine phosphorylation of insulin receptor and insulin receptor substrate-1 in rat skeletal muscle. *Acta Physiol Scand*. 2000; 169(2):133–139.
12. Haigis MC, Sinclair DA. Mammalian sirtuins: biological insights and disease relevance. *Annu Rev Pathol*. 2010;5:253–295.
13. Yu J, Auwerx J. Protein deacetylation by SIRT1: an emerging key post-translational modification in metabolic regulation. *Pharmacol Res*. 2010; 62(1):35–41.
14. Boily G, et al. SirT1 regulates energy metabolism and response to caloric restriction in mice. *PLoS One*. 2008;3(3):e1759.
15. Bordone L, et al. SIRT1 transgenic mice show phenotypes resembling calorie restriction. *Aging Cell*. 2007;6(6):759–767.
16. Philp A, et al. Sirtuin 1 (SIRT1) deacetylase activity is not required for mitochondrial biogenesis or peroxisome proliferator-activated receptor-γ coactivator-1α (PGC-1α) deacetylation following endurance exercise. *J Biol Chem*. 2011;286(35):30561–30570.
17. Cheng HL, et al. Developmental defects and p53 hyperacetylation in Sir2 homolog (SIRT1)-deficient mice. *Proc Natl Acad Sci U S A*. 2003; 100(19):10794–10799.
18. Rodgers JT, Lerin C, Haas W, Gygi SP, Spiegelman BM, Puigserver P. Nutrient control of glucose homeostasis through a complex of PGC-1alpha and SIRT1. *Nature*. 2005;434(7029):113–118.
19. Vaziri H, et al. hSIR2(SIRT1) functions as an NAD-dependent p53 deacetylase. *Cell*. 2001; 107(2):149–159.
20. Luo J, et al. Negative control of p53 by Sir2alpha promotes cell survival under stress. *Cell*. 2001; 107(2):137–148.
21. Nemoto S, Fergusson MM, Finkel T. SIRT1 functionally interacts with the metabolic regulator and transcriptional coactivator PGC-1α. *J Biol Chem*. 2005; 280(16):16456–16460.
22. Abell K, et al. Stat3-induced apoptosis requires a molecular switch in PI(3)K subunit composition. *Nat Cell Biol*. 2005;7(4):392–398.
23. Argentino DP, Dominici FP, Munoz MC, Al-Regaiey K, Bartke A, Turyn D. Effects of long-term caloric restriction on glucose homeostasis and on the first steps of the insulin signaling system in skeletal muscle of normal and Ames dwarf (Prop1df/Prop1df) mice. *Exp Gerontol*. 2005;40(1–2):27–35.
24. Argentino DP, Munoz MC, Rocha JS, Bartke A, Turyn D, Dominici FP. Short-term caloric restriction does not modify the in vivo insulin signaling pathway leading to Akt activation in skeletal muscle of Ames dwarf (Prop1(df)/Prop1(df)) mice. *Horm Metab Res*. 2005;37(11):672–679.
25. Argentino DP, Dominici FP, Al-Regaiey K, Bonkowski MS, Bartke A, Turyn D. Effects of long-term caloric restriction on early steps of the insulin-signaling system in mouse skeletal muscle. *J Gerontol A Biol Sci Med Sci*. 2005;60(1):28–34.
26. Gazdag AC, Dumke CL, Kahn CR, Cartee GD. Calorie restriction increases insulin-stimulated glucose transport in skeletal muscle from IRS-1 knockout mice. *Diabetes*. 1999;48(10):1930–1936.
27. Song XM, Ryder JW, Kawano Y, Chibalin AV, Krook A, Zierath JR. Muscle fiber type specificity in insulin signal transduction. *Am J Physiol*. 1999; 277(6 pt 2):R1690–R1696.
28. Taniguchi CM, Emanuelli B, Kahn CR. Critical nodes in signalling pathways: insights into insulin action. *Nat Rev Mol Cell Biol*. 2006;7(2):85–96.
29. Terauchi Y, et al. Increased insulin sensitivity and hypoglycaemia in mice lacking the p85 alpha subunit of phosphoinositide 3-kinase. *Nat Genet*. 1999;21(2):230–235.
30. Mauvais-Jarvis F, et al. Reduced expression of the murine p85alpha subunit of phosphoinositide 3-kinase improves insulin signaling and ameliorates diabetes. *J Clin Invest*. 2002;109(1):141–149.
31. Ueki K, et al. Positive and negative roles of p85 alpha and p85 beta regulatory subunits of phosphoinositide 3-kinase in insulin signaling. *J Biol Chem*. 2003;278(48):48453–48466.
32. Chen D, et al. p50alpha/p55alpha phosphoinositide 3-kinase knockout mice exhibit enhanced insulin sensitivity. *Mol Cell Biol*. 2004;24(1):320–329.
33. Luo J, et al. Loss of class IA PI3K signaling in muscle leads to impaired muscle growth, insulin response, and hyperlipidemia. *Cell Metabolism*. 2006; 3(5):355–366.
34. Nie Y, et al. STAT3 inhibition of gluconeogenesis is downregulated by SirT1. *Nat Cell Biol*. 2009; 11(4):492–500.
35. Pfeffer LM, Mullersman JE, Pfeffer SR, Murti A, Shi W, Yang CH. STAT3 as an adapter to couple phosphatidylinositol 3-kinase to the IFNAR1 chain of the type I interferon receptor. *Science*. 1997; 276(5317):1418–1420.
36. Uddin S, et al. Interferon-dependent activation of the serine kinase PI 3′-kinase requires engagement of the IRS pathway but not the Stat pathway. *Biochem Biophys Res Commun*. 2000;270(1):158–162.
37. Fröjdö S, et al. Phosphoinositide 3-kinase as a novel functional target for the regulation of the insulin signaling pathway by SIRT1. *Mol Cell Endocrinol*. 2011;335(2):166–176.
38. Sun C, et al. SIRT1 improves insulin sensitivity under insulin-resistant conditions by repressing PTP1B. *Cell Metab*. 2007;6(4):307–319.
39. Sato S, Fujita N, Tsuruo T. Modulation of Akt kinase activity by binding to Hsp90. *Proc Natl Acad Sci U S A*. 2000;97(20):10832–10837.
40. Sundaresan NR, et al. The deacetylase SIRT1 promotes membrane localization and activation of Akt and PDK1 during tumorigenesis and cardiac hypertrophy. *Sci Signal*. 2011;4(182):ra46.
41. Banks AS, et al. SirT1 gain of function increases energy efficiency and prevents diabetes in mice. *Cell Metab*. 2008;8(4):333–341.
42. Canto C, et al. AMPK regulates energy expenditure by modulating NAD+ metabolism and SIRT1 activity. *Nature*. 2009;458(7241):1056–1060.
43. Canto C, et al. Interdependence of AMPK and SIRT1 for metabolic adaptation to fasting and exercise in skeletal muscle. *Cell Metab*. 2010;11(3):213–219.
44. Gonzalez AA, Kumar R, Mulligan JD, Davis AJ, Weindruch R, Saupe KW. Metabolic adaptations to fasting and chronic caloric restriction in heart, muscle, and liver do not include changes in AMPK activity. *Am J Physiol Endocrinol Metab*. 2004;287(5):E1032–E1037.
45. Palacios OM, et al. Diet and exercise signals regulate SIRT3 and activate AMPK and PGC-1alpha in skeletal muscle. *Aging (Albany NY)*. 2009;1(9):771–783.
46. Jiang W, Zhu Z, Thompson HJ. Dietary energy restriction modulates the activity of AMP-activated protein kinase, Akt, and mammalian target of rapamycin in mammary carcinomas, mammary gland, and liver. *Cancer Research*. 2008;68(13):5492–5499.
47. Edwards AG, Donato AJ, Lesniewski LA, Gioscia RA, Seals DR, Moore RL. Life-long caloric restriction elicits pronounced protection of the aged myocardium: a role for AMPK. *Mech Ageing Dev*. 2010; 131(11–12):739–742.
48. Shinmura K, Tamaki K, Saito K, Nakano Y, Tobe T, Bolli R. Cardioprotective effects of short-term caloric restriction are mediated by adiponectin via activation of AMP-activated protein kinase. *Circulation*. 2007;116(24):2809–2817.
49. Gazdag AC, et al. Lower calorie intake enhances muscle insulin action and reduces hexosamine levels. *Am J Physiol Regul Integr Comp Physiol*. 2000; 278(2):R504–R512.
50. Saberi M, et al. Hematopoietic cell-specific deletion of toll-like receptor 4 ameliorates hepatic and adipose tissue insulin resistance in high-fat-fed mice. *Cell Metab*. 2009;10(5):419–429.
51. Karnieli E, Zarnowski MJ, Hissin PJ, Simpson IA, Salans LB, Cushman SW. Insulin-stimulated translocation of glucose transport systems in the isolated rat adipose cell. Time course, reversal, insulin concentration dependency, and relationship to glucose transport activity. *J Biol Chem*. 1981; 256(10):4772–4777.
52. Barbour LA, et al. Human placental growth hormone increases expression of the p85 regulatory unit of phosphatidylinositol 3-kinase and triggers severe insulin resistance in skeletal muscle. *Endocrinology*. 2004;145(3):1144–1150.